A Novel Speed Controller of Ultra-High-Speed PMSM for A-Mechanically-Based-Antenna (AMEBA)

Kazi Nishat Tasnim
Department of Electrical and Computer Engineering
Mississippi State University
Starkville, MS-39762, USA
kt1446@msstate.edu

Md. Khurshedul Islam
Department of Electrical and Computer Engineering
Mississippi State University
Starkville, MS-39762, USA
mi264@msstate.edu

Moinul Shahidul Haque
Controls Engineer
Nexteer Automive
Saginaw, Michigan 48601-9494
US
moinul.haque@nexteer.com

Seungdeog Choi
Department of Electrical and Computer Engineering
Mississippi State University
Starkville, MS-39762, USA
seungdeog@ece.msstate.edu

2022 IEEE Applied Power Electronics Conference and Exposition (APEC) | 978-1-6654-0688-8/22/$31.00 ©2022 IEEE | DOI: 10.1109/APEC43599.2022.9773724

***Abstract*— A robust and anti-disturbance speed controller for an ultra-high-speed permanent magnet synchronous machine (UHS-PMSM) is proposed to assist A Mechanically Based Antenna (AMEBA) in an RF-denied environment such as underwater and underground facilities. A 2kW, 8.33kHz, high-power-density UHS-PMSM is designed for operating the AMEBA. Robust high-speed control of this motor is crucial for an accurate transmission of the signal. However, motor performance and system stability deteriorate due to parameter variation at increased temperature and frequency. To address these issues, a novel fast Anti-Disturbance Sliding Mode-based Deadbeat Model Predictive (ADSM-DMP) control is proposed for precise speed control and to minimize the effect of dynamic parameter variation. The proposed controller achieves 47.7% faster settling time, 96.7% reduction in average torque fluctuation, and 12.46% reduced total harmonic distortion (THD) in current. For experimentally validating the proposed controller, cascode GaN-FET based inverter is designed to operate in high frequency and high-temperature regions.**

Keywords—Ultra-High-Speed Permanent Magnet Synchronous Motor (UHS-PMSM), Anti-Disturbance Sliding Mode-based Deadbeat Model Predictive Control (ADSM-DMP), Reaching law, GaN-FET based inverter, TI DSP F28335.

I. Introduction

PMSMs are extensively used in intricate mechatronic systems for their high-power factor, efficiency, and power density. PMSMs are also popular for operating in a wide speed range with optimum dynamic torque response [1]-[2], motivating a UHS-PMSM for AMEBA applications [3]. In AMEBA, the load of UHS_PMSM, a magnetic dipole is used to transmit ULF/VLF (0.3kHz to 10kHz) magnetic field as a communication signal in RF-denied, under the earth-surface, and into deep-sea infrastructures [4]. [5] and [18] contains the design of the UHS-PMSM for driving AMEBA. As the rotational speed of magnet dipole will define the quality of the transmission signal, accurate speed control, and smooth torque response of the UHS-PMSM are crucial. A high frequency, high-power density, highly efficient and portable motor drive is

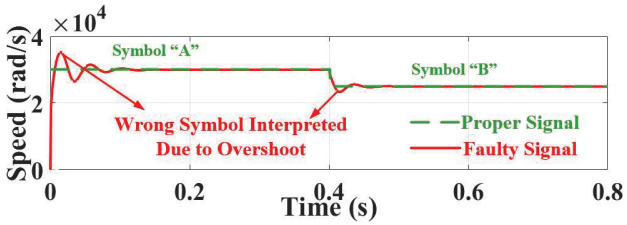

Fig.1: Demonstration of a transmission signal

required for the motor . A receiver might misinterpret the message due to the higher error rate of the received signal as shown in Fig. 1. Thus, transmitted signal should be clear and fast according to receiver's specification. For this purpose, motor speed must be regulated carefully to achieve minimum settling time and overshoot. However, UHS-PMSM faces stability and performance issues due to the gradual non-linearity with the increasing fundamental frequency [8]. So, critical speed control issues are motor parameter variation, change in load torque, and system stability at high bandwidth.

A rigorous literature review [6] - [19] has been done to check the existing controllers' performance with the requirements of AMEBA. Proportional Integral (PI) controllers are traditionally popular for simple implementation and better steady-state response. However, gain values cannot be changed once the system starts to operate. So, fixed gain values limit its capability to adapt to disturbances, such as load torque change and parameter variation. In [7] and [19], self-tuned PIs with Fuzzy Logic is implemented to adapt with load torque variation. In [6], a disturbance observer-based PI controller was designed to improve the transient behavior of PI under disturbances and

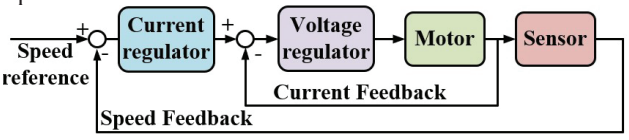

Fig.2: Existing double loop controller

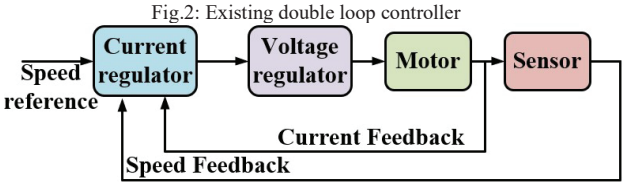

Fig. 3: Proposed controller with single bandwidth

Authorized licensed use limited to: Mississippi State University Libraries. Downloaded on June 28,2022 at 20:34:49 UTC from IEEE Xplore. Restrictions apply.

uncertainties. Although these modified PI controllers can improve the performance under load torque change, there is no discussion about model parameter variation and high-speed operation. Also, with increasing speed, the motor model becomes more non-linear, so, the linearized PI controller cannot perform efficiently.

For addressing these issues, various non-linear control methods, such as, sliding mode, model predictive, backstepping, Kalman filter are used for motor drives. Among these methods, sliding mode control (SMC) showed better performances with parameter variations, load torque change and other external disturbances [8] - [16]. In [8] and [13], terminal sliding mode control is incorporated to make the states reach the sliding surface within finite time. However, for rejecting disturbance, high switching gain has to be incorporated that can cause huge chattering. Chattering is one of the major drawbacks of SMC [10]. In [11], a higher-order sliding mode is established to address this drawback, but computational complexity increases with increasing order. Authors in [14], proposed a "quick reaching law approach" that can associate an adaptive switching gain to limit both disturbance and chattering. Although, this approach results in desirable response in low frequency, chattering increases in higher frequency as, it is related with sampling time. For solving this limitation, authors in [12] proposed sliding mode-based extended state observer (SMESO) and in [15] extended sliding mode disturbance observer (ESMDO) is proposed. However, in these articles, only the load torque change is taken as a state of ESO. In [16], hyperbolic ESO is incorporated to estimate lumped disturbances, including external and internal uncertainties and load torque. Using these methods, disturbance can be estimated and fed forward to SMC, that can eliminate the tradeoff between anti-disturbance and chattering property of the controller.

However, most of the literatures discussed above, focuses on the speed control loop, and PI is employed for the current control loop. The double control loop, as shown in Fig. 2, imposes a tradeoff between settling time and transient response. This tradeoff limits the existing controllers' ability to attain the required speed for AMEBA. Furthermore, a high proportional gain coefficient is required for high-frequency operation, which increases the system's bandwidth. And, high bandwidth leads to instability according to the Nyquist stability criterion.

For addressing these tradeoffs of anti-disturbance-chattering and settling time-overshoot, a fast-Anti-disturbance Sliding Mode-based Deadbeat Model Predictive Control (ADSM-DMP) is proposed for UHS-PMSM speed control. The proposed controller addresses both the chattering and uncertainites. A modified fast double power reaching law is proposed for faster response with lesser chattering. Whereas, for compensating for the load torque change, parameter variation, and other uncertainties, a non-linear Gudermannian function-based ESO (GFESO) is developed. Gudermannian function allows faster and smoother switching of ADSM that contributes to chattering reduction and better steady state response. At the same time, tracking differential (TD) is designed to limit overshoot. So, the combination of GFESO, TD and fast reaching law based SMC is able to address the tradesoff mentioned above. DMP, the voltage regulator, is cascaded with ADSM to enable the system to operate with a single bandwidth, as shown in Fig. 3. Estimated speed and sensed current are fed back to the current regulator.

Table I

REFERENCE SPEED

Central frequency	Frequency Deviation	Speed Reference(rpm)	Symbol
1kHz	25Hz	57000	A
		60000	B
		63000	C

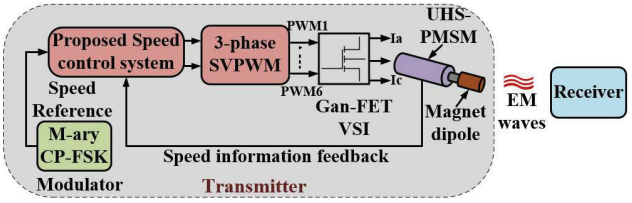

Fig.4: High-level AMEBA system

However, the voltage regulator uses model predictive control, that eliminates the need of current feed-back allowing the controller to work with a single loop which ensures better stability in high frequency. Thus, the proposed ADSM-DMP can cope with disturbances and, simultaneously, ensures stability in the high-speed region. A Lyapunov stability criterion is utilized to ensure closed-loop stability of the system and to establish bounded values for gains.

The rest of the paper is organized as follows. Section II relates the AMEBA requirement with the UHS-PMSM speed profile. Section III contains a brief discussion about UHS-PMSM. In section IV, ADSM-DMP is validated and finally, section V concludes the paper with summarized results.

II. CONTROL REQUIREMENT FOR UHS-PMSM

Fig. 4 illustrates the concept of the AMEBA system, which shows that the reference speed of the motor is associated with the data modulation scheme of the transmitted message. In [3] and [4], the modulation scheme for the transmitter of AMEBA is discussed in details. M-ary continuous phase-frequency shift keying (M-ary CP-FSK) is proposed for power-efficient data transmission that can reduce the average torque requirement of the UHS-PMSM. Here, $M$is the modulation order of CP-FSK that represents the number of possible signals. Each symbol is associated with a certain frequency, which is used as the reference speed of the motor so that the magnetic dipole can transmit a magnetic field with the same frequency.

CP-FSK has a central frequency, f_c and a frequency deviation, Δf. Frequencies to be transmitted are defined as $f_i = f_c + (2i - 1 - M)\Delta f$, where $i = 1,2,\dots,M$. Range of central frequency, f_c is chosen from 25Hz to 3kHz. Frequency deviation, Δf, is kept between 4Hz to 25Hz to avoid interference with the power system signal of 60Hz and its harmonics. Frequency deviation should be kept as low as possible to keep the rate of motor speed change under a certain value to satisfy the rated power and rated torque of the UHS-PMSM. For smooth transmission of symbols, overshoot of motor speed should be less than $(\Delta f/f_c)\%$ and settling time, T_{stl} should be less than one-fourth of the symbol period required by the receiver [4]. In Table I, reference speed for different symbol are represented.

Authorized licensed use limited to: Mississippi State University Libraries. Downloaded on June 28,2022 at 20:34:49 UTC from IEEE Xplore. Restrictions apply.

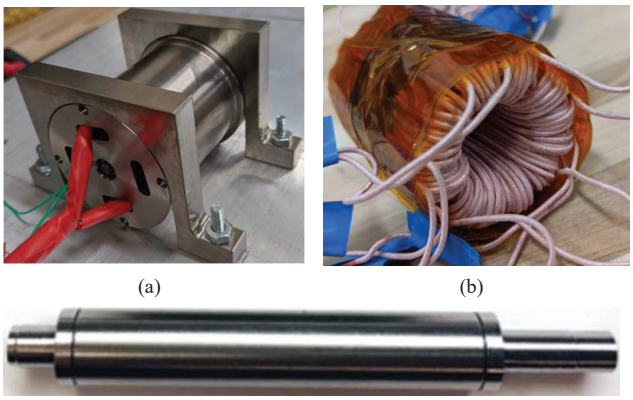

(a) (b)

(c)

Fig.5: (a) Prototype of UHS-PMSM with (b) the stator (c) and rotor

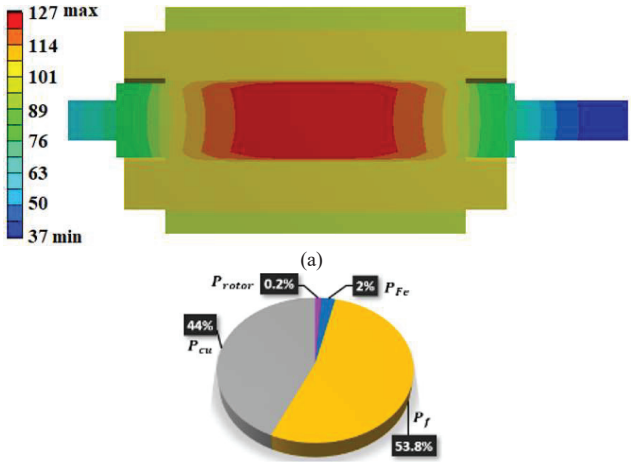

(a)

(b)

Fig.6: (a) Rotor axial temperature at rated condition and (b) percentage of losses due to temperature increase.

III. UHS-PMSM Model

A UHS-PMSM of 2kW rated power and 8.333kHz fundamental frequency is designed in [18]. A prototype in Fig. 5 is designed to increase power efficiency and provide rated torque, allowing the motor to have 38.2mNm torque.

The rotor of the UHS-PMSM has a cylindrical magnet inside a hollow retaining sleeve. Since the flux path is equal in both d-and q-axis orientation, stator inductance along direct axis,L_d and along quadrature axis, L_q are equal. Due to high power density, rotor axial temperature varies, as shown in Fig. 6(a). With varying temperatures, motor parameters such as, stator resistance and mutual flux linkage change. And it causes loss of the system as Fig. 6(b). This phenomenon can be addressed with the proposed control method. Specification of the motor are shown in Table II.

Table. II
UHS-PMSM MODEL PARAMETER

Parameter	Symbol	Value
Stator Resistance	R	0.1382
Stator Inductance	$L_d = L_q$	65×10^{-6}
Flux Linkage	λ_{pm}	.0032
Inertial Coefficient	J	3.8×10^{-6}
Friction Coefficient	B	2×10^{-7}
Rated Power	P_{rated}	2kW
Rated Current	I_{rated}	3.9A
Rated Load Torque	T_l	38.9mNm

Mathematical model of the UHS-PMSM is given in (1) where, v_d is d-axis voltage, v_q is q-axis voltage. i_d is d-axis current, i_q is q-axis current and T_e is electrical torque of the motor.

$$\begin{aligned} v_d &= Ri_d + L_d\frac{di_d}{dt} - L_q P\omega_m i_q \\ v_q &= Ri_q + L_q\frac{di_q}{dt} + L_d P\omega_m i_d + \lambda_{pm} P\omega_m \\ Te &= 1.5P\lambda_{pm} i_q \end{aligned} \quad (1)$$

IV. Fast ADSM Based DMP Control

A. Novel Fast Reaching Law for Sliding Mode Control

"Reaching Law" approach is adopted for robust control purpose for its characteristic of guiding the system states to the sliding surface for fast and chattering free response [14]. Conventional exponent reaching laws are expressed as,

$$\frac{ds}{dt} = -a_1\, sgn(s) - a_2\, s; \qquad a_1, a_2 > 0 \quad (2)$$

where, s is the sliding surface, a_1 and a_2 are constants. It is evident from (2), reaching the speed of the system state is higher when the error is away from the surface, s, but it gradually reduces as it reaches closer to the surface. Once the states reach the surface, the first term of (2) contributes to keeping them on the surface, but as it is a discontinuous function, the states fluctuate within a band which is called quasi-sliding-mode-band (QSMB). QSMB, Δ_1 of (2) is,

$$\Delta_1 = 2\frac{a_1 T}{1 - a_2 T} \quad (3)$$

where T is the sampling time. QSMB is constant in this case, and this property introduces chattering in the system. For reducing chattering, the authors of [16] proposed an adaptive reaching law. Proposed reaching law, novel quick reaching law (NQRL) reduces the chattering, but on the other hand, reaching time increases. Increased reaching time results in increased settling time of the system, which is not acceptable for AMEBA applications. For solving this tradeoff, a novel fast reaching law is proposed in this paper as,

$$\frac{ds}{dt} = -a_1|s|^{f1}\, sgn(s) - a_2|s|^{f2} s \quad (4)$$

where $f1 = tanh(s^{\sigma 1}) - 1.6\, arctan(e^{\sigma 2 s}) + \lambda_o$ and, $f2 = \sigma_3\, tanh(\lambda_1|s|)$. In this reaching law, $a_1, a_2, \sigma_1, \sigma_2$ *and* λ_1 are defined to be positive and greater than one and $\lambda_o = \frac{\pi}{2} + \sigma_3$, where $0 < \sigma_3 < 1$. In the proposed reaching law, the coefficient of the discontinuous term is defined as an adaptive function. When, $|s| > 1$, coefficient of the second term in (4) is responsible for increasing the reaching speed as $f_2 > 0$. And the coefficient of the first term is responsible when $|s| < 1$ as,$f_1 < 0$. QSMB of the proposed reaching law, Δ_2 is,

$$\Delta_2 = 2\frac{a_1 T|s(n)|^{f_1}}{1 - a_2 T|s(n)|^{f2}} \quad (5)$$

where, n is the sample number. The QSMB is a function of the nth sample of $|s|$ .Which means, the band will reduce as it gradually reaches zero error position. Fig. 7 demonstrates the

Authorized licensed use limited to: Mississippi State University Libraries. Downloaded on June 28,2022 at 20:34:49 UTC from IEEE Xplore. Restrictions apply.

comparison between the two abovementioned QSMBs. Gradually decreasing the QSMB of the proposed reaching law contributes to reducing the chattering of the system. At the same time, a higher reaching speed reduces settling time as well.

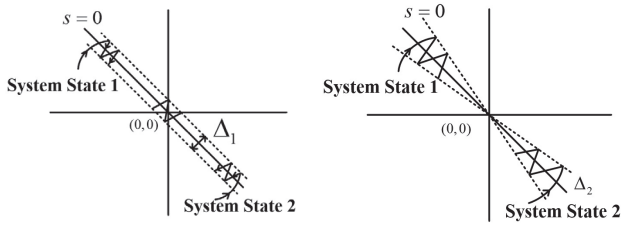

Fig.7: Comparison of QSMB Δ_1 *and* Δ_2 in phase portrait.

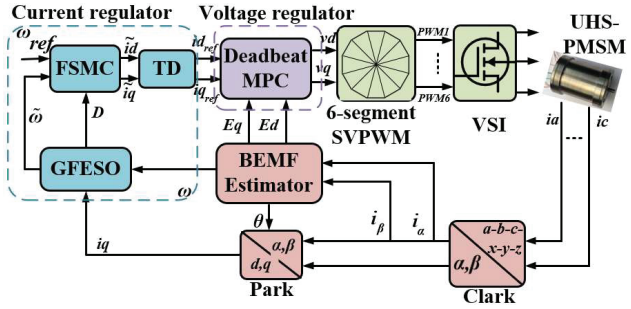

Fig.8 Novel Fast ADSM-DMP speed controller

B. *Novel Fast ADSM-DMP Controller*

The proposed control system, ADSM-DMP, utilizes sliding mode control for current regulation and model predictive control for voltage regulation. The current and voltage regulator works sequentially, and the computations are sample-based. Fig. 8 shows the overall control diagram. From Fig. 8, it is seen that the current regulator consists of three segments. The first segment is Gudermannian function-based extended state observer (GFESO). GFESMO estimates the uncertainties or disturbances such as load torque change and parameter variation. Once the disturbance is estimated, the estimated speed response is optimized by compensating for the disturbance. From the motor model, speed and torque can be defined as,

$$\dot{\omega} = Xi_q - Y\omega - ZT_l \tag{6}$$

where $X = (3P\lambda_{pm})/J$, $Y = B/J$, and $Z = 1/J$ Now, if disturbances and uncertainties are considered, (6) becomes,

$$\dot{\omega} = (X + \Delta X)i_q - (Y + \Delta Y)\omega - (Z + \Delta Z)T_l \tag{7}$$

If disturbance, D is defined as, $D = \Delta X i_q - \Delta Y\omega - (Z + \Delta Z)T_l$, then, (7) can be simplified as,

$$\omega = Xiq - Y\omega + D \tag{8}$$

D is estimated based on the Gudermannian function, and estimated speed of the motor is optimized as (9).

$$\begin{aligned} \dot{d} &= -\xi_1\left(2\,arctan(e^{4e_1}) - \frac{\pi}{2}\right) \\ \dot{\tilde{\omega}} &= Xi_q - Y\tilde{\omega} - \xi_2 e_1 + d \\ e_1 &= \tilde{\omega} - \omega \end{aligned} \tag{9}$$

where d is the tracked disturbance and $\tilde{\omega}$ is the compensated speed. ξ_1 *and* ξ_2 depend on the stability of the system, which will be discussed later.

Now, the second segment, the fast sliding mode controller (FSMC) is used to calculate the current reference command utilizing the compensated motor speed. The sliding surface is chosen as,

$$s = err + C\int_0^t err(\tau)d\tau \tag{10}$$

Where, $err = \omega_{ref} - \tilde{\omega}$ and ω_{ref} is the reference speed of the system. Now, from (4), (9), and (10), reference q-axis current command can be calculated as,

$$\begin{aligned} \tilde{\imath}_q = \big(\dot{\omega}_{ref} + Y\tilde{\omega} - D + a_1|s|^{f1}\,sgn(s) + a_2|s|^{f2}s \\ + C(err)\big)/X \end{aligned} \tag{11}$$

Finally, third segment, tracking differential (TD) is used to compensate for the overshoot in $\tilde{\imath}_q$ to reduce output speed overshoot. Finally, i_{qref} using TD is designed as,

$$\frac{di_{qref}}{dt} = -\xi_3\left|i_{qref} - \tilde{\imath}_q\right| arctan\left(e^{4(i_{qref} - \tilde{\imath}_q)}\right) - \frac{\pi}{2} \tag{12}$$

where $\xi_3 > 0$. In this controller, the d-axis current is kept as zero to get maximum torque response.

Now, for voltage regulator segment, deadbeat model predictive (DMP) controller is cascaded with a sliding mode controller. The model predictive controller uses the present current sample to predict future voltage values according to (1) and regulates the output optimally. DMP is designed by discretizing v_q as,

$$\begin{aligned} v_q = e^{\frac{\tau_s R}{L}}\left(i_{qref}(n+1) - \left(R\left(1 - e^{-\frac{\tau_s R}{L}}\right)\right)^{-1} i_{qref}(n)\right) \\ + E_q \end{aligned} \tag{13}$$

where, τ_s is the sampling time.

As mentioned before, this cascaded configuration allows the controller to work with a single bandwidth, ω_{bw} represented as (14).

$$\omega_{bw} = 2\pi\left(\int_0^t \left(-a_1|s|^{f1}\,sgn(s) - a_2|s|^{f2}s\right)^{-1} dt\right)^{-1} \tag{14}$$

C. *Stability Analysis of FSMC*

The stability of the system depends on the coefficient of the disturbance. So ξ_1 *and* ξ_2 should be bounded to protect stability. For analyzing system stability, Lyapunov function id used, and it is selected considering the energy of a system as, $V = \frac{1}{2}s^2$. So, $\dot{V} = s\dot{s}$ and for stability, $\dot{V} < 0$. Solving this inequality, it can be defined that, $\xi_1 + \xi_2 < 2000$.

V. Simulation and Experimental Validation

In this section, the proposed ADSM-DMP controller is verified through simulation and experiment. The superiority of the proposed single loop controller to the traditional dual loop controllers in terms of stability is discussed. Moreover, the

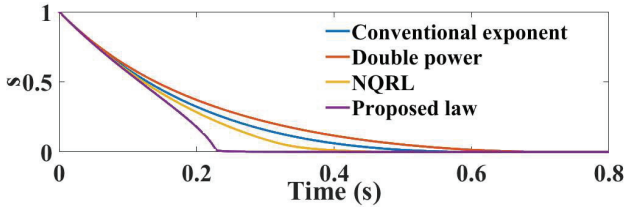

Fig. 9: Sliding surface vs. time

Authorized licensed use limited to: Mississippi State University Libraries. Downloaded on June 28,2022 at 20:34:49 UTC from IEEE Xplore. Restrictions apply.

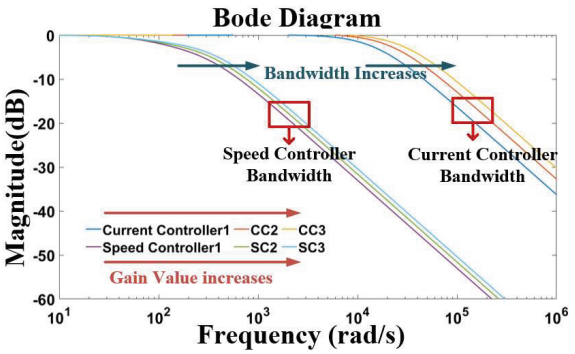

Fig.10: Bandwidth comparison with increasing gain values.

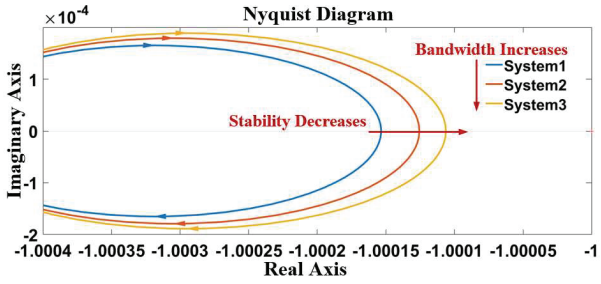

Fig.11: Increasing instability with increasing bandwidth.

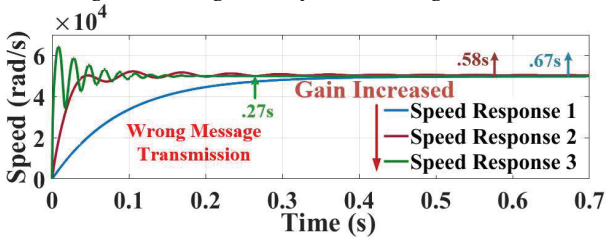

Fig.12: Comparison of speed response with Traditional dual loop controller for reducing settling time.

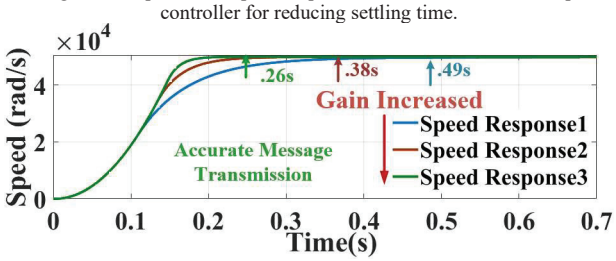

Fig.13: Comparison of speed response with ADSM-DMP controller for reducing settling time.

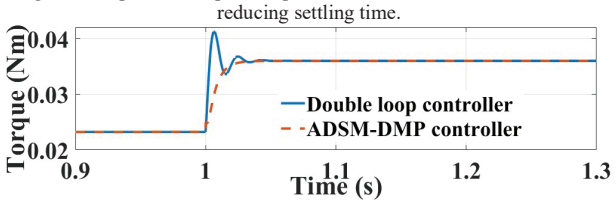

Fig.14: Comparison of output torque when T_l is changed from 23mNm to 36mNm at 1s.

ability of the proposed controller to address parameter variation and external disturbances is also verified.

A. Simulation Results

1) Single loop Vs. Dual loop controller stability

Table. III
SPEED AND TEMPERATURE MAPPING OF UHS-PMSM FROM FEA

Speed (rpm)	Coil Temperature (℃)	Magnet Temperature (℃)
50000	76	51
200000	90	68
350000	100.6	95
500000	118	130

The proposed controller is implemented using MATLAB-Simulink. At first, the proposed novel reaching law (4) is validated compared to the existing laws, described in subsection A of section IV. It is observed that the convergence rate is improved by 47.7%, which eventually will contribute to improving the setting time of the whole system. Fig. 9 shows a faster performance of the proposed law than the NQRL, power reaching law and conventional exponent reaching law as described in (2).

As stated before, the proposed controller consists of single bandwidth and this bandwidth also depends on the reaching law of the controller. Mathematically, bandwidth of the whole system is as (12). Whereas, for traditional dual loop controller, bandwidth of the current control loop is 20 times broader than the speed control loop. Initially, zero of the speed controller's transfer function should be at, $-\frac{J}{B} = -19$ and zero of the current controller's transfer function should be at $-\frac{R}{L} = -2126$, in order to maintain first order system, which is necessary for avoiding oscillation. But, for achieving required settling time and overshoot for AMEBA, gain values has to be tuned. As the gain values increases, the bandwidths increase as shown in Fig 10. And with increasing bandwidth, Nyquist diagram reaches the value -1, which is the stability margin (Fig. 11). So, it can be concluded that, dual loop controllers cannot provide expected response while operating in high speed region and the trade off between settling time and overshoot deteriorates the AMEBA response.

2) Perfomance of motor under different conditions

For executing AMEBA application properly, speed response of the motor has to maintain a certain control constraint. Settling time and overshoot of the speed response depends on the frequency deviation (Δf) and central frequency (f_c). In the worst-case scenario, settling time should be less than 0.3s, and overshoot should be less than $(\Delta f / f_c)\%$, that can go as low as .05%. If the speed response does not satisfy the control constraints, one transmitted signal might interfere with the next transmitted signal, eventually resulting in the wrong message transmission. Satisfying the control requirements becomes difficult by applying the traditional dual loop controller, as there is a tradeoff between settling time and overshoot of the output response. Fig. 12 shows the comparison of speed responses with increasing gain for maintaining the required response. However, the gain has to be increased for reducing settling time, which results in increased overshoot. Moreover, increased gain also makes the system vulnerable to instability, as discussed in the previous subsection. From Fig. 12, it is evident that, in an attempt to reduce the settling time, the overshoot increases. Settling time reduces from 0.67s to 0.27s, tuning the gain values, but at the same time, overshoot increases

Authorized licensed use limited to: Mississippi State University Libraries. Downloaded on June 28,2022 at 20:34:49 UTC from IEEE Xplore. Restrictions apply.

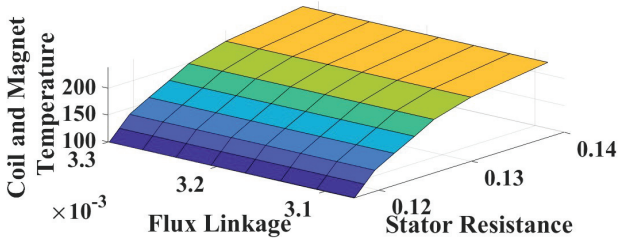

Fig.15: R and λ_{pm} variation with coil and magnet temperature

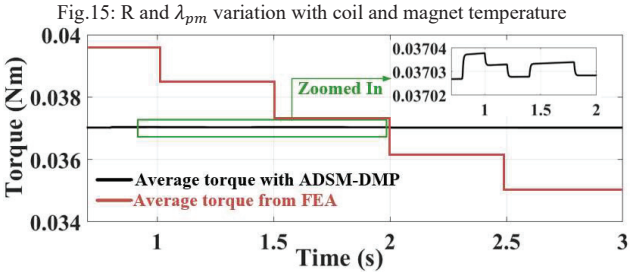

Fig.16: Average torque variation under parameter variation

up to 28.5%. According to Fig. 12, speed response 1 is not fast enough, and speed response 2 and 3 have a large overshoot, making the receiver read the wrong frequency or message. Whereas applying the proposed ADSM-DMP single loop controller, the settling time of speed response is improved from .49s to .26s, without any overshoot (Fig. 13). Also, Fig. 14 shows the comparison of torque response of the motor with both controllers. Load torque, T_l, is changed from 23mNm to 36mNm at 1s time. With a double loop controller, overshoot is 13.88%, whereas with ADSM-DMP, overshoot is negligible. These characteristics of the controller allow the motor to transmit an accurate signal to the receiver.

Another control constraint is to maintain the output torque. As the motor has to rotate a magnetic dipole, the torque response must have to be stable. However, being a high-power density (>60kW/L) motor, the temperature of the magnet tends to rise from 51℃ to 130℃, when the speed increases from

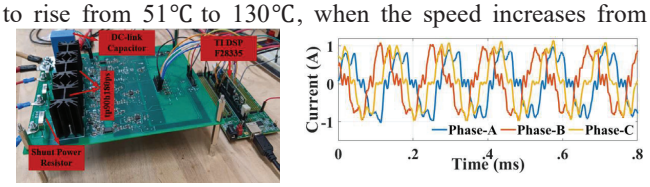

(a) (b)

Fig.17: (a) Cascode GaN-FET inverter and (b) current profile of the inverter.

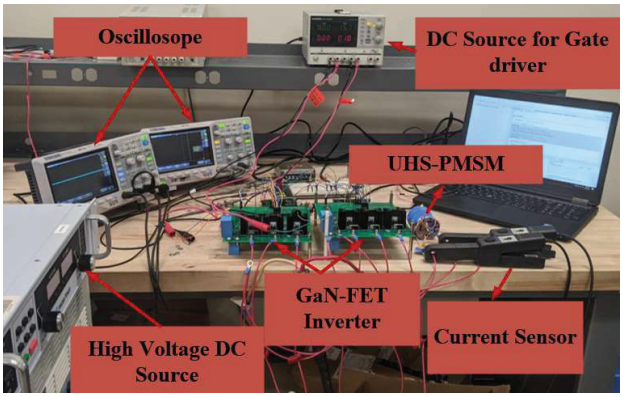

Fig.18: Experimental setup

50000rpm to 500000rpm (Table III). In rear earth magnets, like, Sm_2Co_{17}, magnetic remanence (B_r) and intrinsic coercivity (H_c) are temperature dependent, maintaining $B_r = 1 - \alpha(T - 20℃)$ and $H_c = 1 - \beta(T - 20℃)$ equations, where α and β are material dependent. As permanent magnet flux linkage, λ_{pm} is a function of B_r and H_c, it will decrease with increasing temperature, which will eventually distort the average torque. Fig. 15 shows the variation of stator resistance with coil temperature and variation of λ_{pm} with magnet temperature. From FEA simulation, it is observed that, at a fixed speed, temperature of magnet can rise up to 240℃. And, average torque can vary from 38.6mNm to 35.9mNm as a consequence of varying λ_{pm} with temperature. As the average torque variation is not acceptable for AMEBA, GFESO is designed in the controller to track the disturbance and to reduce the torque variation. In Simulink, parameter variation has been designed after .5s, and Figure 16 shows that average torque variation reduces from 2.65mNm to 0.02mNm.

B. Experimental validation

For evaluating the proposed controller and for operating the UHS-PMSM prototype, a three-phase inverter with a current and voltage sensor has been designed and validated. As

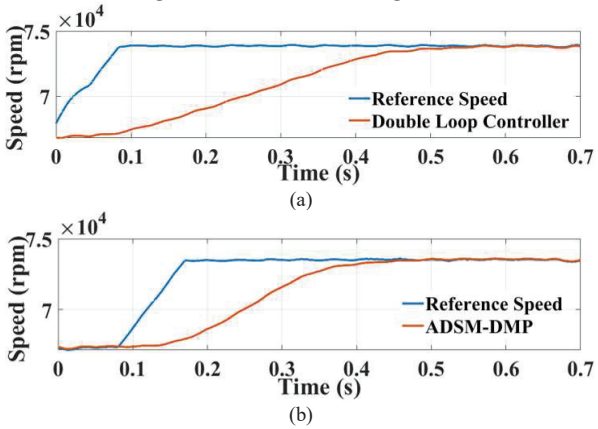

(a)

(b)

Fig.19: Speed response of UHS-PMSM at 73k rpm with (a) double-loop controller and (b) proposed ADSM-DMP controller

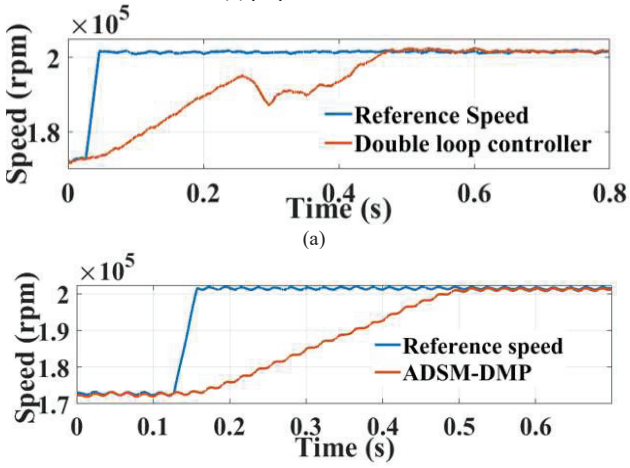

(a)

(b)

Fig.20: Speed response of UHS-PMSM at 230k rpm with (a) double-loop controller and (b) proposed ADSM-DMP controller

Authorized licensed use limited to: Mississippi State University Libraries. Downloaded on June 28,2022 at 20:34:49 UTC from IEEE Xplore. Restrictions apply.

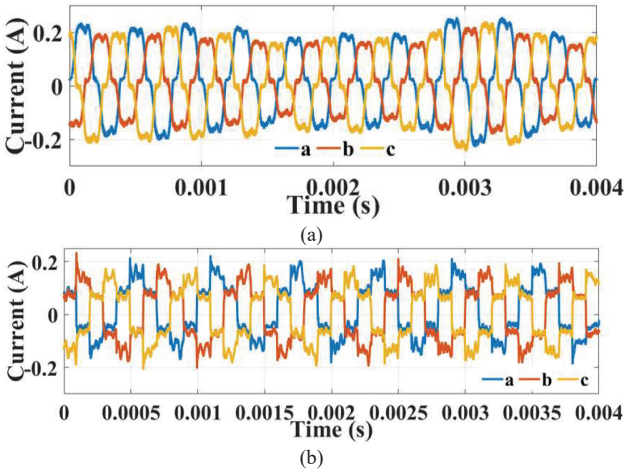

Fig.21: Phase current of UHS-PMSM with (a) traditional double loop controller and (b) proposed ADSM-DMP controller

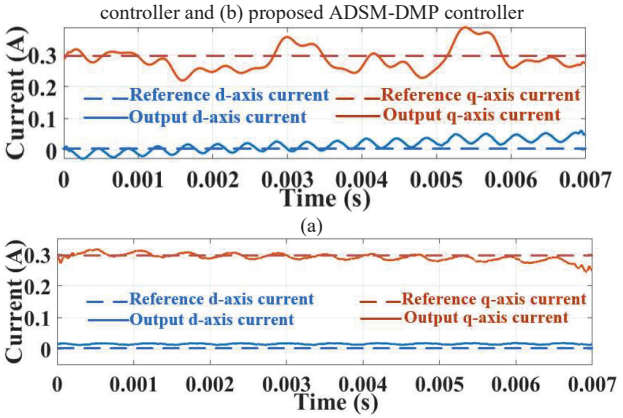

Fig.22: d-q axis current profile of UHS-PMSM with (a) traditional double loop controller and (b) proposed ADSM-DMP controller

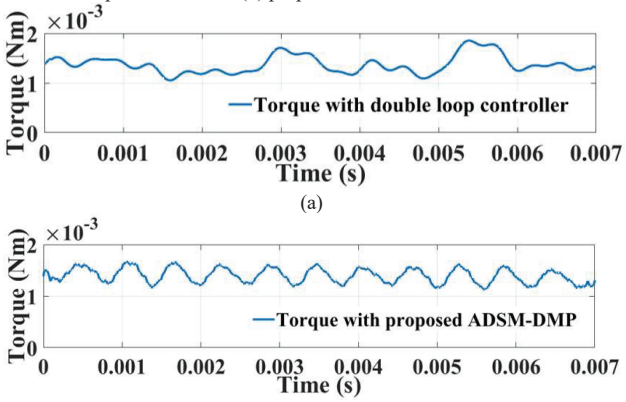

Fig.23: Torque response of UHS-PMSM with (a) traditional double loop controller and (b) proposed ADSM-DMP controller

the rated frequency of the motor is 8.33kHz, the switching frequency of the inverter would reach to 200kHz. Wide bandgap (WBG) switches, such as Gallium Nitride (GaN) and Silicon Carbide (SiC), can operate in this high-frequency range. Cascode GaN-FET, TP90H180PS, was chosen for the inverter for its ability to operate at high frequency and ease of integration. For close loop control of the motor, an isolated amplifier, AMC1301 is used for sensing current. The 3-phase inverter has been validated for 90% rated fundamental frequency and with 120kHz switching frequency. 10uH inductor was used as line inductance The phase current of the inverter is shown in Fig. 17(b). The system is controlled using a TI DSP F28335 as shown in Fig. 17(a). The experimental setup is as shown in Fig. 18.

For AMEBA application, the speed of the motor should be able to change rapidly, maintaining the control constraints as discussed in section II. For experimental validation, UHS-PMSM is operated in two ranges of speeds (0.15 rated and 0.50 rated).

In the first condition, the reference speed is changed to 73k rpm. Fig. 19 shows the speed response of UHS-PMSM with the traditional double-loop controller and proposed ADSM-DMP controller. In this speed range, both of the controllers behave optimally. However, the traditional controller takes 0.54s to settle down, whereas the proposed method takes 0.36s to reach a steady state. For the second condition, the reference speed was changed to 230k rpm. Fig. 20 compares the speed response with both controllers. It is observed that, traditional controllers show significant fluctuation in speed response. As, in this speed range motor parameters start to fluctuate according to FEA simulation. However, speed response with the proposed controller shows more promising results. Settling time improves by 33.33% and steady-state response improves from 0.2423% to 0.598%.

To observe the torque response of the UHS-PMSM under traditional and proposed controller, the motor was operated at 230k rpm and 7% rated load. Fig. 21 shows the three-phase current of the UHS motor with a traditional controller and ADSM-DMP controller. Current amplitude fluctuates with existing controllers, whereas ADSM-DMP shows more consistent current. From Fig. 22, the d-q axis current with both controllers is compared. Its observed that q-axis current ripple decreases from 55.6% to 23.2% with using the proposed

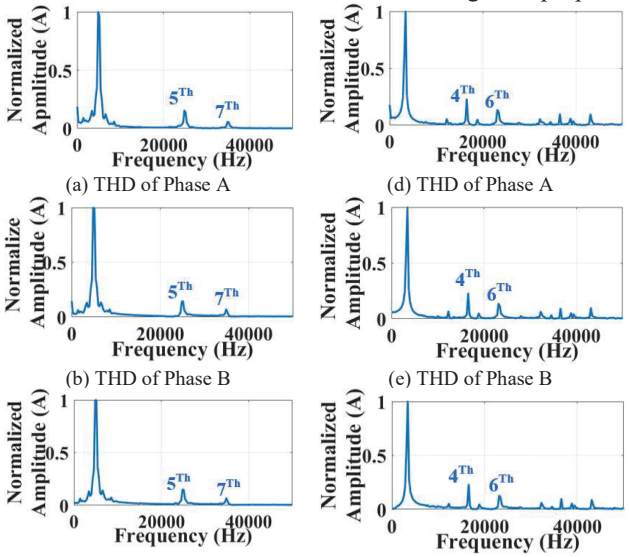

Fig.24: THD Comparison of UHS-PMSM phase current with (a, b, c) double-loop controller and (d, e, f) ADSM-DMP controller

Authorized licensed use limited to: Mississippi State University Libraries. Downloaded on June 28,2022 at 20:34:49 UTC from IEEE Xplore. Restrictions apply.

controller. Moreover, Fig. 23 shows that the proposed controller can reduce the torque ripple from 55.39% to 24%.

Total harmonic distortion (THD) of the phase current is analyzed for comparison, as shown in Fig. 24. With the existing controller, 5^{th} and 7^{th} harmonics dominate in the THD calculation. With the proposed controller, the odd harmonics (5^{th} and 7^{th}) are reduced. THD is improved by 12.46% with the proposed ADSM-DMP controller. Table IV shows the comparison of THD of each phase with both controllers.

So, from simulation and experimental results, it can be concluded that, the proposed controller works better for AMEBA system, in terms of settling time, and overshoot of speed, average torque fluctuation and torque ripple, than the existing controllers.

Table. IV
TOTAL HARMONIC DISTORTION (THD) COMPARISON

Control Scheme	THD (%)		
	Phase A	Phase B	Phase C
Double loop	16.86	17.1	16.82
ADSM-DMP	13.3	14.2	13.9

VI. CONCLUSION

In this paper, a robust speed controller, ADSM-DMP of UHS-PMSM is proposed for the AMEBA. Gudermannian function based fast ESO has been proposed for disturbance estimation which reduces the average torque fluctuation from 2.65mNm to 0.02mNm under parameter variation and load torque change. A novel fast reaching law has been established to reduce the settling time by 47.7%. Tracking Differential (TD) has been incorporated for reducing the overshoot from 28.6% to almost 0%. Deadbeat model predictive control is used for voltage regulation which ensures the stability in the higher frequency region as, it allows the system to work with a single bandwidth. Experimental validation shows that, settling time reduces by 33.33%. Torque ripple reduces from 55.39% to 24%, and THD of each phase of current improves by 12.46%. Thus, the better performance of the proposed controller, ADSM-DMP than the existing double loop controllers is validated for maintaining the control constarints imposed by the AMEBA.

ACKNOWLEDGEMENT

This research is supported by the National Science Foundation (NSF) CCSS-Comms Circuits and Sens System Program (Award# 1905434).

REFERENCE

[1] G. Wu, S. Huang, Q. Wu, F. Rong, C. Zhang and W. Liao, "Robust Predictive Torque Control of N*3-Phase PMSM for High-Power Traction Application," in IEEE Transactions on Power Electronics, vol. 35, no. 10, pp. 10799-10809, Oct. 2020.

[2] S. Morimoto, Y. Tong, Y. Takeda and T. Hirasa, "Loss minimization control of permanent magnet synchronous motor drives," in IEEE Transactions on Industrial Electronics, vol. 41, no. 5, pp. 511-517, Oct. 1994.

[3] J. S. Glickstein, J. Liang, S. Choi, A. Madanayake and S. Mandal, "Power-Efficient ELF Wireless Communications Using Electro-Mechanical Transmitters," in IEEE Access, vol. 8, pp. 2455-2471, 2020.

[4] M. T. B. Tarek et al., "Power-Efficient Data Modulation for All-Mechanical ULF/VLF Transmitters," 2018 IEEE 61st International Midwest Symposium on Circuits and Systems (MWSCAS), 2018, pp. 759-762.

[5] M. K. Islam and S. Choi, "Rotordynamic Analysis of 500 000 r/min 2 kW Ultra-High-Speed Machine for Portable Mechanical Antenna," 2021 IEEE International Electric Machines & Drives Conference (IEMDC), 2021.

[6] R. Errouissi, A. Al-Durra and S. M. Muyeen, "Experimental Validation of a Novel PI Speed Controller for AC Motor Drives With Improved Transient Performances," in IEEE Transactions on Control Systems Technology, vol. 26, no. 4, pp. 1414-1421, July 2018.

[7] Gou-Jen Wang, Chuan-Tzueng Fong and K. J. Chang, "Neural-network-based self-tuning PI controller for precise motion control of PMAC motors," in IEEE Transactions on Industrial Electronics, vol. 48, no. 2, pp. 408-415, April 2001.

[8] S. Li, M. Zhou and X. Yu, "Design and Implementation of Terminal Sliding Mode Control Method for PMSM Speed Regulation System," in IEEE Transactions on Industrial Informatics, vol. 9, no. 4, pp. 1879-1891, Nov. 2013.

[9] H. Pan, G. Zhang, H. Ouyang and L. Mei, "A Novel Global Fast Terminal Sliding Mode Control Scheme for Second-Order Systems," in IEEE Access, vol. 8, pp. 22758-22769, 2020.

[10] G. P. Incremona, M. Rubagotti, M. Tanelli and A. Ferrara, "A General Framework for Switched and Variable Gain Higher Order Sliding Mode Control," in IEEE Transactions on Automatic Control, vol. 66, no. 4, pp. 1718-1724, April 2021.

[11] F. Dinuzzo and A. Ferrara, "Higher Order Sliding Mode Controllers With Optimal Reaching," in IEEE Transactions on Automatic Control, vol. 54, no. 9, pp. 2126-2136, Sept. 2009.

[12] W. Xu, A. K. Junejo, Y. Liu, M. G. Hussien and J. Zhu, "An Efficient Antidisturbance Sliding-Mode Speed Control Method for PMSM Drive Systems," in IEEE Transactions on Power Electronics, vol. 36, no. 6, pp. 6879-6891, June 2021.

[13] H. Wang et al., "Continuous Fast Nonsingular Terminal Sliding Mode Control of Automotive Electronic Throttle Systems Using Finite-Time Exact Observer," in IEEE Transactions on Industrial Electronics, vol. 65, no. 9, pp. 7160-7172, Sept. 2018.

[14] H. Pan, G. Zhang, H. Ouyang and L. Mei, "A Novel Global Fast Terminal Sliding Mode Control Scheme for Second-Order Systems," in IEEE Access, vol. 8, pp. 22758-22769, 2020.

[15] X. Zhang, L. Sun, K. Zhao and L. Sun, "Nonlinear Speed Control for PMSM System Using Sliding-Mode Control and Disturbance Compensation Techniques," in IEEE Transactions on Power Electronics, vol. 28, no. 3, pp. 1358-1365, March 2013.

[16] Y. Wang, Y. Feng, X. Zhang and J. Liang, "A New Reaching Law for Antidisturbance Sliding-Mode Control of PMSM Speed Regulation System," in IEEE Transactions on Power Electronics, vol. 35, no. 4, pp. 4117-4126, April 2020.

[17] P. Cortes, M. P. Kazmierkowski, R. M. Kennel, D. E. Quevedo and J. Rodriguez, "Predictive Control in Power Electronics and Drives," in IEEE Transactions on Industrial Electronics, vol. 55, no. 12, pp. 4312-4324, Dec. 2008.

[18] Md Khurshedul Islam, Seungdeog Choi, "Multiphysics Optimization Model to Design High-Power Ultra-High Speed Machine for Portable Mechanical Antenna Application", in press.

[19] C. Wang and Z. Q. Zhu, "Fuzzy Logic Speed Control of Permanent Magnet Synchronous Machine and Feedback Voltage Ripple Reduction in Flux-Weakening Operation Region," in IEEE Transactions on Industry Applications, vol. 56, no. 2, pp. 1505-1517, March-April 2020

Authorized licensed use limited to: Mississippi State University Libraries. Downloaded on June 28,2022 at 20:34:49 UTC from IEEE Xplore. Restrictions apply.